Supplementary materials

Enhanced removal of oxytetracycline from aquatic solution using MnO_x@Fe_3O_4 bimetallic nanoparticle coated powdered activated carbon: synergism of adsorption and chemical autocatalytic oxidation processes

Jiahui Zhou [a,*], Shu Wang [b]

[a] State Key Laboratory of Pollution Control and Resources Reuse, School of Environmental Science and Engineering, Tongji University, Shanghai, 200092, PR China

[b] Department of Pharmaceutics, Nagasaki University Graduate School of Biomedical Sciences, Nagasaki University, Nagasaki, 852-8501, Japan

* Corresponding author. E-mail address: zhoujiahui1991@126.com (J. Zhou)

7 Tables
9 Figures
13 Pages

Text S1

Preparation of MnO_x@Fe_3O_4 bimetallic nanoparticles coated powdered activated carbon (MnO_x@Fe_3O_4-PAC)

The 200 mesh acid-washed PAC was chosen as the carbon matrix for MnO_x@Fe_3O_4-PAC synthesis. 3.9 g $FeCl_3 \cdot 6H_2O$ and 1.4 g $FeCl_2 \cdot 4H_2O$ were dissolved in a beaker with 450 mL ultrapure water at 80℃. 3.3 g PAC was added into the solution, and then 5M NaOH solution was added dropwise (volume: 50 mL; velocity: 10 mL/min) into the suspension, mechanical stirring for 1h, and maturing for 2h. After removing the supernatant, the remains were mixed with 2.3 g $MnCl_2 \cdot 4H_2O$ in the beaker with 400 mL fresh ultrapure water, and temperature was remained at 80℃. The aqueous solution contained 6.0 g/L $KMnO_4$ and 3.0 g/L NaOH was added dropwise (volume: 200 mL; velocity: 10 mL/min) into the suspension, mechanical stirring for 1h, and maturing for 2h. After removing the supernatant, the remains were dried overnight, washed with ultrapure water to neutral pH, freeze-dried and hermetical stored until use. Eventually, MnO_x@Fe_3O_4-PAC was synthesized with a mass ratio of 1/1/2 for MnO_x/Fe_3O_4/PAC.

Text S2

Adsorption isotherms

The Langmuir and Freundlich isotherm models were included as follows:

$$q_e = \frac{K_L q_m C_e}{1 + K_L C_e}$$

$$q_e = K_F C_e^{\frac{1}{n}}$$

where q_e (mg/g) and q_m (mg/g) were the equilibrium adsorption capacity and the maximum adsorption capacity of OTC, respectively; C_e (mg/L) was the equilibrium concentration of OTC; K_L and K_F were the constants of Langmuir and Freundlich, respectively; 1/n was surface heterogeneity or adsorption intensity.

Adsorption kinetics

The pseudo-first order, pseudo-second order, Elovich model, and intraparticle diffusion equations were included as follows:

$$q_t = q_e - q_e e^{-k_1 t}$$

$$q_t = \frac{k_2 {q_e}^2 t}{1 + k_2 q_e t}$$

$$q_t = \frac{1}{\beta_E} \ln \frac{\alpha_E}{\beta_E} + \frac{1}{\beta_E} \ln t$$

$$q_t = k_{id} t^{\frac{1}{2}} + L$$

where q_e (mg/g) and q_t (mg/g) were the adsorption capacity of OTC at the equilibrium time and time t, respectively; k_1 (min^{-1}) was the pseudo-first-order model rate constant; k_2 ($g.mg^{-1}.min^{-1}$) was the pseudo-second-order model rate constant; t (min) was the adsorption time; α_E ($mg.g^{-1}.min^{-1}$) and β_E ($g.mg^{-1}$) were Elovich constants; k_{id} ($mg.g^{-1}.min^{-0.5}$) was the intraparticle diffusion rate.

Adsorption thermodynamics

The adsorption thermodynamic equations were included as follows:

$$\Delta G^0 = -RT \ln K_D$$

$$K_D = \frac{C_A}{C_e}$$

$$\ln K_D = \frac{\Delta S^0}{R} - \frac{\Delta H^0}{RT}$$

where ΔG^0 ($kJ.mol^{-1}$), ΔH^0($kJ.mol^{-1}$), and ΔS^0 ($kJ.mol^{-1}.K^{-1}$) were Gibbs free energy, standard enthalpy, and standard entropy, respectively; R was the universal gas constant (8.314 $J.mol^{-1}.K^{-1}$); C_A and C_e were the concentration of OTC in the solid phase and the liquid phase at the equilibrium time, respectively; T (K) was the temperature.

Text S3

Analysis of OTC and Intermediates

The residual concentration of OTC was determined using high-performance liquid chromatography (HPLC) with a Zorbax Eclipse XDB-C18 column (4.6 mm × 150 mm, 5 μm, Agilent, USA) on an Agilent 1200 Infinity system. The mobile phase consisted of a mixture of sodium dihydrogen phosphate solution (0.01 mol/L) and acetonitrile (80:20, v/v). The column temperature was set at 35 °C, and the mobile phase flow rate was maintained at 1

mL/min. A sample injection volume of 10 μL was used, and detection was performed at a wavelength of 268 nm.

The intermediates of OTC were identified using ultra-performance liquid chromatography-mass spectrometry (UPLC-MS) on an Agilent 1290 UPLC system coupled with a Q-TOF 6550 mass spectrometer (Agilent, USA). The mobile phase consisted of a mixture of formic acid solution (0.1%, m/m) and acetonitrile (90:10, v/v). The column temperature was set at 40°C, and the injection volume was 5 μL. The mobile phase flow rate was maintained at 0.3 mL/min. ESI (electrospray ionization) in positive ion mode was used for the estimation of OTC and its intermediates.

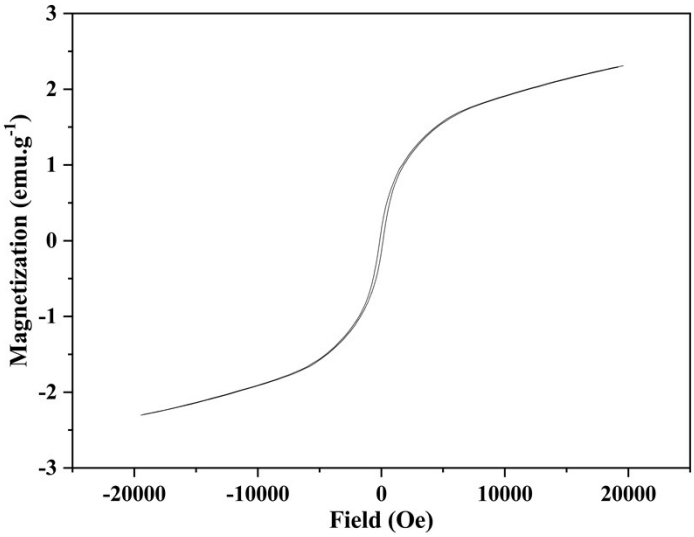

Fig. S1. VSM magnetization curves of MnO_x@Fe_3O_4-PAC.

Table S1. Aperture parameters of PAC and MnO_x@Fe_3O_4-PAC.

Sample	BET specific surface area /$m^2.g^{-1}$	BJH total pore volume /$mL.g^{-1}$	Macropore volume /$mL.g^{-1}$	Mesopore volume /$mL.g^{-1}$	Micropore volume /$mL.g^{-1}$
PAC	347.54	0.25	0.03	0.12	0.10
MnO_x@Fe_3O_4-PAC	222.89	0.37	0.04	0.27	0.06

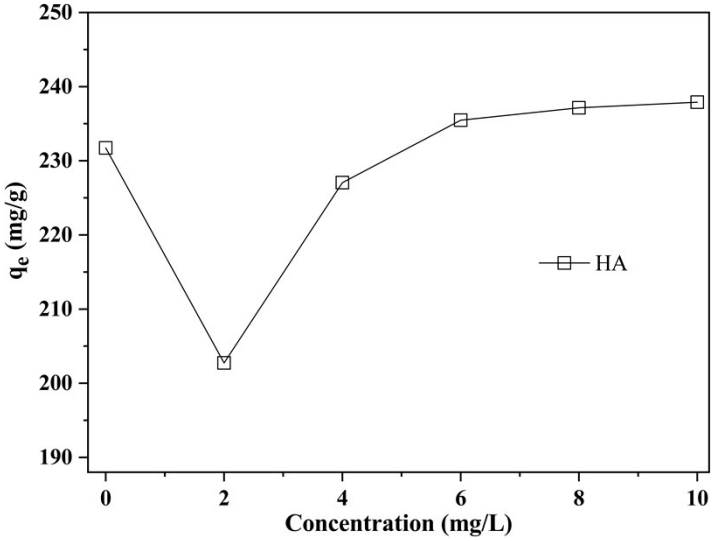

Fig. S2. Effect of HA on OTC adsorption on MnO_x@Fe_3O_4-PAC. Reaction conditions: OTC_0 = 150 ppm, MnO_x@Fe_3O_4-PAC dosage = 0.5 g/L, initial pH = 3.

Table S2. The parameters of Langmuir and Freundlich isotherms for the adsorption of OTC on PAC and MnO_x@Fe_3O_4-PAC.

Sample	Langmuir isotherms $q_e = \frac{K_L q_m C_e}{1 + K_L C_e}$			Freundlich isotherms $q_e = K_F C_e^{\frac{1}{n}}$		
	q_m	K_L	R^2	K_F	n	R^2
PAC	285.558	0.598	0.832	111.041	4.146	0.979
MnO_x@Fe_3O_4-PAC	284.800	0.063	0.915	47.159	2.574	0.973

Table S3. The maximal adsorption capacity of OTC on different adsorbents.

Adsorption materials	**q_m (mg/g)**	**Isotherm model**	**References**
MnO_x@Fe_3O_4-PAC	231.7	Freundlich	This Study
zeolite/Fe_3O_4	27.1	Langmuir	1
Fe_3O_4-HA-La	23.4	Redlich-Peterson	2
Surfactant-modified-alumina	143.0	two-step model	3
Multi-walled carbon nanotubes	73.0	Freundlich	4
Polyaniline coated peanut shells	65.5	Langmuir	5
Graphene oxide functionalized magnetic particles	45.0	Langmuir	6

Table S4. Parameters of adsorption kinetic models of OTC on MnO_x@Fe_3O_4-PAC.

C/ mg.L^{-1}	$q_{e,max}$/ mg.g^{-1}	pseudo-first-order model			pseudo-second-order model			Elovich model			Intra-particle diffusion model			
		$q_{e,cal}$	k_1	R^2	$q_{e,cal}$	k_2	R^2	α_E	β_E	R^2	k_{stage1}	R^2	k_{stage2}	R^2
75	111.659	101.893	0.084	0.942	108.753	0.0012	0.983	1.831	0.079	0.999	5.236	0.976	2.026	0.946
150	189.654	168.645	0.084	0.936	180.693	0.0007	0.974	0.768	0.046	0.994	13.270	0.968	4.494	0.972
225	240.528	218.003	0.081	0.949	233.256	0.0006	0.985	0.628	0.036	0.998	16.524	0.961	4.771	0.964
300	293.270	259.400	0.088	0.934	277.289	0.0005	0.975	0.689	0.031	0.997	17.488	0.965	6.792	0.997

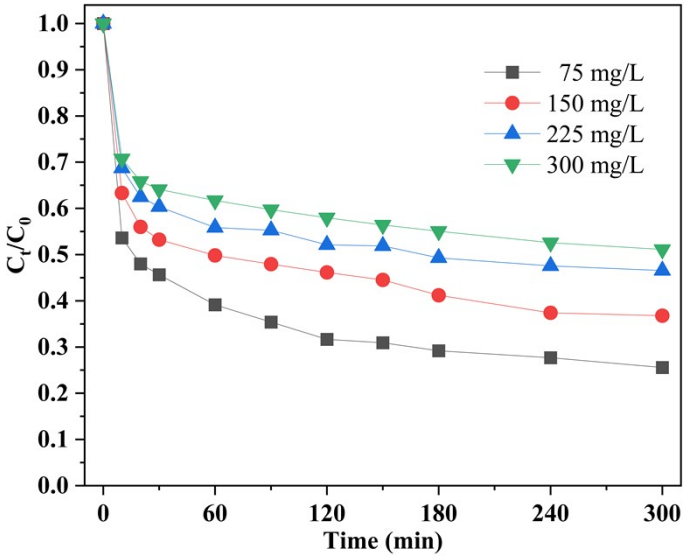

Fig. S3. OTC removal efficiency of MnO_x@Fe_3O_4-PAC at different initial OTC concentrations.

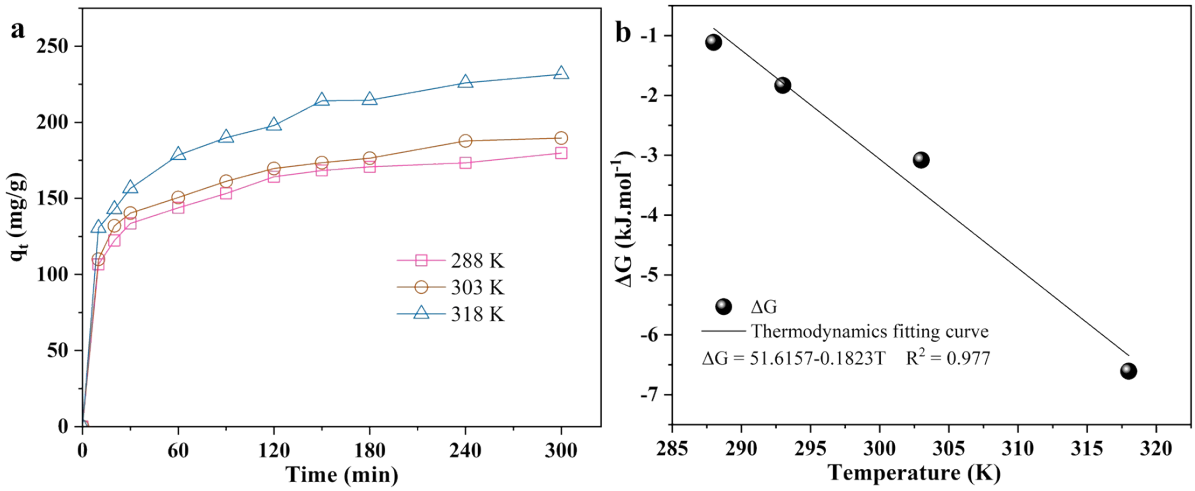

Fig. S4. The influence of temperature (a); and the thermodynamic fitting curve (b) for OTC adsorption on MnO_x@Fe_3O_4-PAC. Reaction conditions: OTC_0 = 150 ppm, MnO_x@Fe_3O_4-PAC dosage = 0.5 g/L, initial pH = 3.

Table S5. Thermodynamic parameters for the adsorption of OTC on MnO_x@Fe_3O_4-PAC.

T/K	ΔG^0/(kJ·mol^{-1})	ΔH^0/(kJ·mol^{-1})	ΔS^0/(kJ·(mol·K)$^{-1}$)
288	-1.11		
293	-1.83	51.62	0.18
303	-3.08		
318	-6.61		

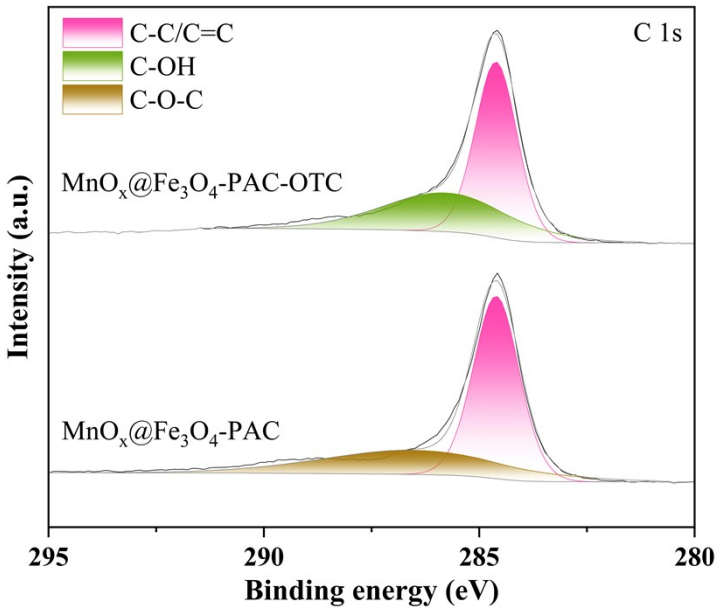

Fig. S5. XPS spectra of C 1s for MnO_x@Fe_3O_4-PAC before and after reaction.

Table S6. XPS results for the relative atomic percentages of C 1s on MnO_x@Fe_3O_4-PAC before and after reaction.

Sample	C-C/C=C	C-OH	C-O-C
MnO_x@Fe_3O_4-PAC	65.4%	n.d.	34.6%
MnO_x@Fe_3O_4-PAC-OTC	59.8%	40.2%	n.d.

Compared with MnO_x@Fe_3O_4-PAC before reaction, the states of C 1s were significantly changed in MnO_x@Fe_3O_4-PAC after reaction, the peak of C-O-C (286.5 eV) disappeared and new peak of C-OH (285.8 eV) appeared, indicating the surface properties of MnO_x@Fe_3O_4-PAC changed during the reaction.

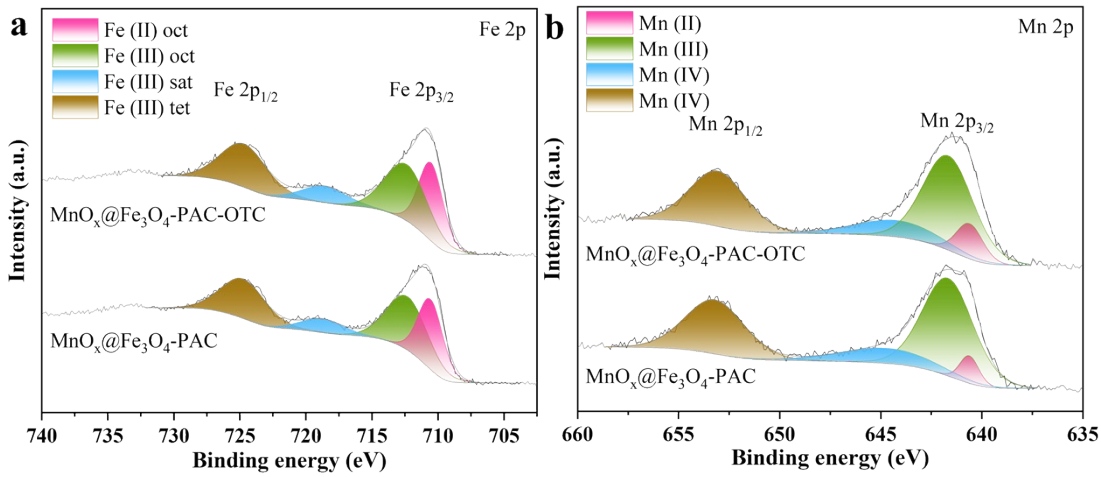

Fig. S6. XPS spectra of Fe 2p (a) and Mn 2p (b) for $MnO_x@Fe_3O_4$-PAC before and after reaction.

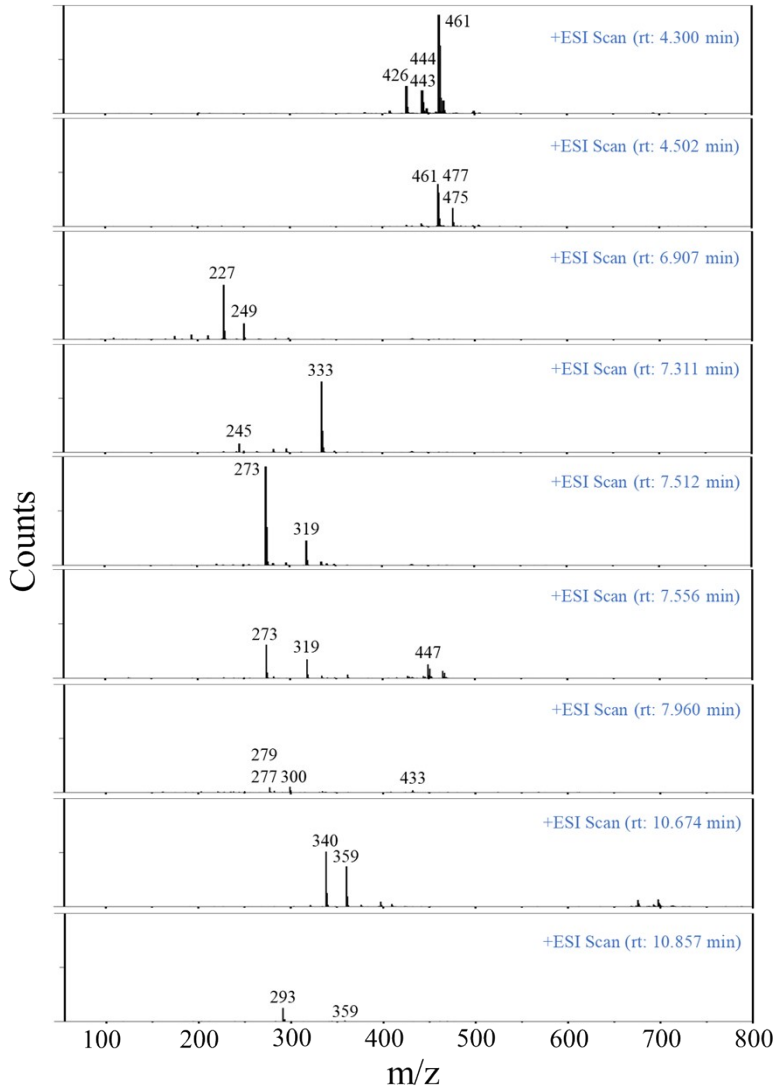

Fig. S7. MS spectra of intermediates generated during the chemical autocatalytic oxidation process.

Table S7. Potential intermediates identified in the chemical autocatalytic oxidation process.

Compound	$[M+H]^+$	Molecular structural formula
OTC	461	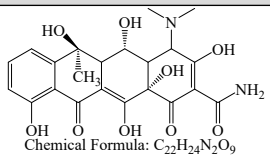 Chemical Formula: $C_{22}H_{24}N_2O_9$ m/z: 461
1	443	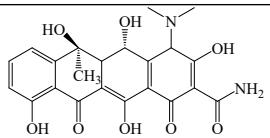 Chemical Formula: $C_{22}H_{22}N_2O_8$ m/z: 443
2	477	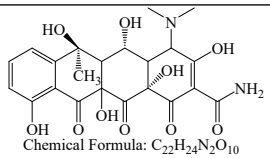 Chemical Formula: $C_{22}H_{24}N_2O_{10}$ m/z: 477
3	443	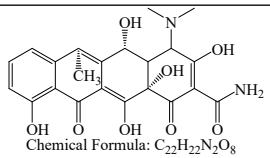 Chemical Formula: $C_{22}H_{22}N_2O_8$ m/z: 443
4	447	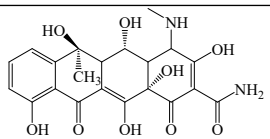 Chemical Formula: $C_{21}H_{22}N_2O_9$ m/z: 447
5	444	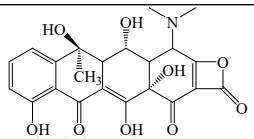 Chemical Formula: $C_{22}H_{21}NO_9$ m/z: 444
6	433	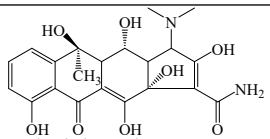 Chemical Formula: $C_{21}H_{24}N_2O_8$ m/z: 433
7	300	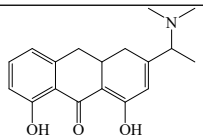 Chemical Formula: $C_{18}H_{21}NO_3$ m/z: 300
8	340	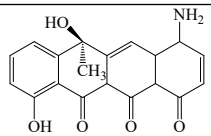 Chemical Formula: $C_{19}H_{17}NO_5$ m/z: 340
9	475	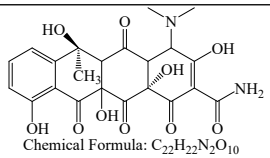 Chemical Formula: $C_{22}H_{22}N_2O_{10}$ m/z: 475

10	293	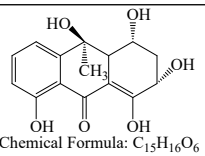 Chemical Formula: $C_{15}H_{16}O_6$ m/z: 293
11	359	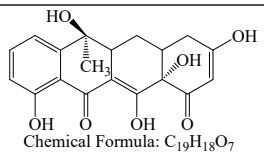 Chemical Formula: $C_{19}H_{18}O_7$ m/z: 359
12	426	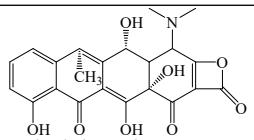 Chemical Formula: $C_{22}H_{19}NO_8$ m/z: 426
13	293	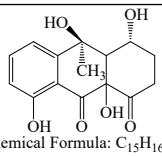 Chemical Formula: $C_{15}H_{16}O_6$ m/z: 293
14	319	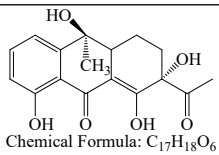 Chemical Formula: $C_{17}H_{18}O_6$ m/z: 319
15	333	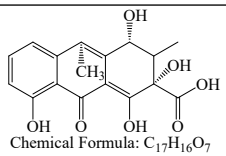 Chemical Formula: $C_{17}H_{16}O_7$ m/z: 333
16	279	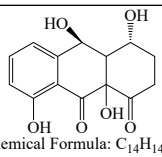 Chemical Formula: $C_{14}H_{14}O_6$ m/z: 279
17	277	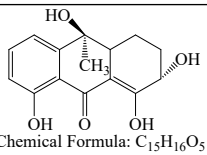 Chemical Formula: $C_{15}H_{16}O_5$ m/z: 277
18	273	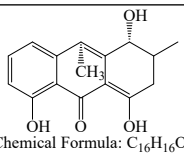 Chemical Formula: $C_{16}H_{16}O_4$ m/z: 273
19	245	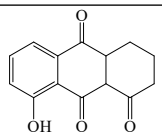 Chemical Formula: $C_{14}H_{12}O_4$ m/z: 245

20	245	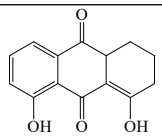 Chemical Formula: $C_{14}H_{12}O_4$ m/z: 245
21	227	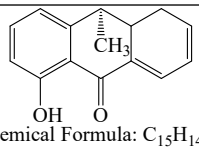 Chemical Formula: $C_{15}H_{14}O_2$ m/z: 227
22	249	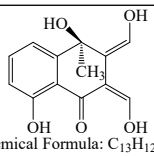 Chemical Formula: $C_{13}H_{12}O_5$ m/z: 249

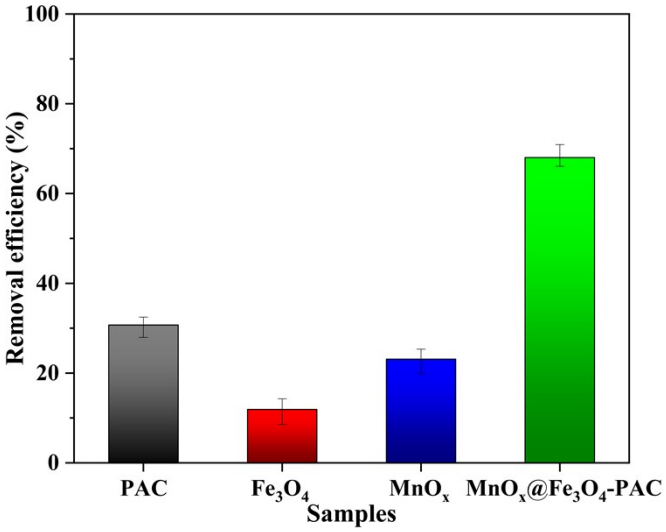

Fig. S8. Comparation of OTC removal contributions of PAC, Fe_3O_4, MnO_x, and MnO_x@Fe_3O_4-PAC.

Text S4

Regeneration of MnO_x@Fe_3O_4-PAC

The experiments were conducted in 500 mL of OTC solution (50 ppm, pH = 3.0) with 0.25 g MnO_x@Fe_3O_4-PAC in a thermostatic mechanical stirring bath at 303 K. After the experiment, MnO_x@Fe_3O_4-PAC was separated from the aqueous solution by outside magnetic field, and then ultrasonically washed five times with 50 mL of methanol. Subsequently, the desorbed MnO_x@Fe_3O_4-PAC was added into fresh OTC solution for the next cycle.

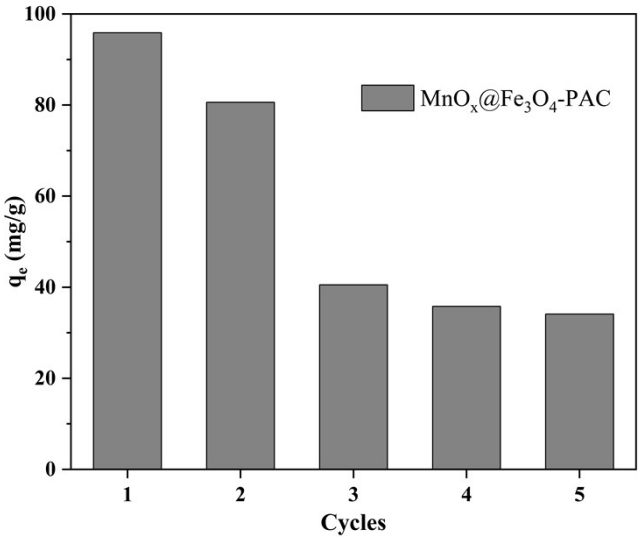

Fig. S9. Regeneration ability of $MnO_x@Fe_3O_4$-PAC for OTC removal.

References

1 G. Başkan, Ü. Açıkel, M. Levent, Investigation of adsorption properties of oxytetracycline hydrochloride on magnetic zeolite/Fe_3O_4 particles, *Adv. Powder Technol.*, 2022, **33**, 103600.

2 C. H. Yan, L. Fan, Y. Chen, Y. T. Xiong, Effective adsorption of oxytetracycline from aqueous solution by lanthanum modified magnetic humic acid, *Colloids Surf. A.*, 2020, **602**, 125135.

3 T. D. Pham, T. T. Tran, V. A. Le, T. T. Pham, T. H. Dao, T. S. Le, Adsorption characteristics of molecular oxytetracycline onto alumina particles: The role of surface modification with an anionic surfactant, *J. Mol. Liq.*, 2019, **287**, 110900.

4 P. Oleszczuk, B. S. Xing, Influence of anionic, cationic and nonionic surfactants on adsorption and desorption of oxytetracycline by ultrasonically treated and non-treated multiwalled carbon nanotubes, *Chemosphere*, 2011, **85**, 1312-1317.

5 F. Belaib, M. Azzedine, B. Boubeker, M. Abdeslam-Hassen, Experimental study of oxytetracycline retention by adsorption onto polyaniline coated peanut shells, *Int. J. Hydrogen Energy*, 2014, **39**, 1511-1515.

6 Y. X. Lin, S. Xu, L. Jia, Fast and highly efficient tetracyclines removal from environmental waters by graphene oxide functionalized magnetic particles, *Chem. Eng. J.*, 2013, **225**, 679-685.